Solar Energy Materials and Solar Cells 188 (2018) 27–36

Contents lists available at ScienceDirect

Solar Energy Materials and Solar Cells

journal homepage: www.elsevier.com/locate/solmat

Light and elevated temperature induced degradation (LeTID) in perovskite solar cells and development of stable semi-transparent cells

The Duong[a,*], YiLiang Wu[a], Heping Shen[a], Jun Peng[a], Shenyou Zhao[a], Nandi Wu[a], Mark Lockrey[b], Thomas White[a], Klaus Weber[a], Kylie Catchpole[a,*]

[a] Research School of Engineering, Australian National University, Canberra 2601, Australia
[b] Australian National Fabrication Facility, Research School of Physics and Engineering, Australian National University, Canberra 2601, Australia

ARTICLE INFO

Keywords:
Perovskite solar cell
Thermal stability
Light stability
Transparent contact
LeTID

ABSTRACT

The stability of perovskite solar cells (PSCs) is one of the major challenges to their commercialization. In this work, the stability of state-of-the-art mesoporous PSCs employing multi-cation mixed-halide perovskite and poly [bis(4-phenyl)(2,4,6-trimethylphenyl)amine] (PTAA) as the hole-transport-layer (HTL) is studied under illumination at an elevated temperature in N_2 environment. The Rb in the quadruple-cation perovskite is found to segregate when the film undergoes aging under simultaneous light and heat exposure. More importantly, the PTAA layer prevents diffusion of gold into the perovskite layer when aged at 85 °C in the dark, but not under light. As a result, the PSCs thermally aged under light degrade much more severely than cells thermally aged in the dark. Therefore, the term Light and elevated Temperature Induced Degradation (LeTID) is introduced for PSCs. The effect is also evident for PCSs employing a copper(II) 2,9,16,23-tetra-tert-butyl-29H,31H-phthalocyanine (CuPC) HTL. This effect seriously impacts the operational stability of PSCs and it might not be detected with the current stress tests defined in the IEC-61646 standard. PSCs with a transparent contact and robust perovskite composition are developed with improved stability against LeTID. The cells retain more than 90% of the initial efficiency after > 160 h operating under illumination at 85 °C in N_2 environment.

1. Introduction

Perovskite solar cells have achieved an efficiency of over 22% after about 9 years of development [1,2]. Moreover, PSCs are suitable as the top cells in a tandem structure with silicon bottom cells as demonstrated in recent work with the record of 27.3% surpassing the record efficiency of single junction silicon solar cells [3–5]. The high efficiency, low cost fabrication and application in tandem with existing technologies show the potential of PSCs in reducing the cost of solar energy. However, stability remains the biggest obstacle to commercialization. PSCs are unstable under many conditions such as light, heat, electrical bias, moisture and oxygen [6]. Great progress has been made to address these stability issues, especially the thermal stability. Notably, semi-transparent PSCs in an inverted (p-i-n) configuration have passed damp heat and thermal cycling tests as defined in the IEC-61646 standard [4]. Carbon-based PSCs have been able to withstand high temperature exposure for three months [7]. Nevertheless, the “normal” (n-i-p) structured mesoporous PSCs currently hold the world record efficiency [2] but their stabilities have been lagging behind. With the commonly used Spiro-MeOTAD as the hole transport layer (HTL), thermal stability is the main issue due to several effects: crystallization of Spiro-MeOTAD at a temperature as low as 85 °C [8], evaporation of the 4-tert-butyl pyridine (tBP) additive [9], and metal diffusion through the layer into the active material [10]. With the replacement of Spiro-MeOTAD by PTAA or CuPC as the HTL, the thermal stability is expected to be significantly enhanced. Shi et al. reported PSCs with the planar structure using formamidinium lead triiodide ($FAPbI_3$) as the absorber and PTAA HTL that are able to pass the damp heat test and thermal cycling with proper encapsulation, though the cell performance is inferior with substantial hysteresis in the study [11]. Kim et al. demonstrated that PSCs employing a CuPC HTL have superior thermal stability even at temperatures as high as 130 °C and good performance of up to 18.8% [12]. These abovementioned studies perform the accelerated tests following the IEC-61646 standards designed for thin film photovoltaic modules. In particular, the cells are thermally aged in the dark (thermal cycling, damp heat) or light soaked at undefined temperatures (outdoor exposure, UV preconditioning) [13]. Photovoltaic modules in the field operate under continuous illumination at high temperature, so this creates a potential gap in testing the reliability of solar cells. Multiple groups have identified a new degradation effect in commercial

* Corresponding authors.
E-mail addresses: the.duong@anu.edu.au (T. Duong), kylie.catchpole@anu.edu.au (K. Catchpole).

https://doi.org/10.1016/j.solmat.2018.08.017
Received 11 June 2018; Received in revised form 20 August 2018; Accepted 22 August 2018
Available online 30 August 2018
0927-0248/

silicon photovoltaic modules using multicrystalline (*mc*-Si) after illumination and elevated temperature, the so called Light and elevated Temperature Induced Degradation (LeTID) effect [14–16]. *mc*-Si silicon modules experience an unexpected drop of 5–10% after a few weeks operating at elevated temperatures (≥ 75 °C). Recently, the LeTID effect has also been observed in silicon modules using Czochralski-grown silicon (Cz-Si) [17] and floatzone silicon (Fz-Si) [18]. PCSs are well known for many instabilities, and therefore it may be that stricter reliability tests are required prior to the commercialization of this technology in order to guarantee performance in the field. Here, we study the thermal stability of mesoporous structure PSCs with multi-cation mixed-halide perovskite with efficiency above 20% both in the dark as well as under illumination, to simulate the actual operating conditions of the device. We find that light has a detrimental effect on the thermal stability of PSCs. This LeTID effect is manifested by two phenomena. First, the Rb in the quadruple-cation perovskite quickly segregates when the film is aged under combined heat and light. More importantly, light activates the diffusion of elemental gold from the rear electrode through the PTAA layer when the device operates at 85 °C. As a result, PSCs thermally aged under light degrade much more severely than PSCs thermally aged in the dark. We find this also applies for PSCs employing a more thermally stable material, CuPC, as the HTL. We note that the degradation mechanisms and response of PSCs in the LeTID effect are remarkably different from silicon solar cells. While the degradation mechanisms of LeTID effect in silicon solar cells are most likely correlating to defects and impurities in the bulk [19,20], the LeTID effect in PSCs is mainly due to the diffusion of metal in the contact into the active material and a change in the material composition to a slight extent. More importantly, the LeTID effect in silicon solar cells features a regeneration process in which the module performance can be recovered while no such regeneration process is found for PSCs in this study. Therefore, we propose that accelerated thermal stress tests should be combined with light exposure to give more insights into the reliability of PSCs. Concurrently, we develop semi-transparent PSCs with a more stable perovskite composition, that are stable for more than 160 h at 85 °C under light.

2. Materials and methods

2.1. Materials

PTAA (M_w 17,700 g mol^{-1}) is purchased from EM Index. Mesoporous transparent titania paste (30 NR-D), formamidinium iodide (FAI) and methylammonium bromide (MABr) are purchased from Dyesol and are used as received. Indium doped zinc oxide target (In_2O_3/ZnO 90/10 wt % and 99.99% purity) is ordered from AJA International. All other materials including titanium(IV) isopropoxide (TTIP) (97% purity), PCBM (99.5% purity), PMMA, dimethylformamide (DMF) (99.8% purity), dimethyl sulfoxide (DMSO) (99% purity), lithium bis(trifluoromethanesulfonyl)imide (Li-TFSI) (99% purity), acetonitrile (99.8% purity), CuPC (99% purity), tBP (96% purity), chlorobenzene (99.8% purity), PbI_2 (99% purity) and $PbBr_2$ (99.999% purity), are purchased from Sigma-Aldrich and are used as received unless specified otherwise.

2.2. Cell fabrication

ITO glass substrates (578274, Sigma Aldrich) are cleaned with detergent, acetone, 2-propanol and ethanol in ultrasonic bath for 10 min each step. A 70 nm-thick TiO_2 blocking layer (cp-TiO_2) is deposited on the clean glass using spin coating the solution of TTIP in 2-propanol at a spin speed of 5000 rpm two times; and the layer is annealed at 500 °C for 30 min in air. 100 nm-thick mesoporous TiO_2 (ms-TiO_2) was deposited on the substrate by spin-coating the solution of TiO_2 paste 30 NR-D in ethanol (1:12 wt ratio) at the spin speed of 5000 rpm. The sample is then annealed at 500 °C in air for 30 min. After cooling down to room temperature, the sample is immediately transferred to a N_2-filled glove box. A mixture of PCBM/PMMA with a ratio of 3:1 in chlorobenzene is spun on the substrates at the speed of 4000 rpm/s and annealed at 100 °C for 10 min. Details on how to prepare the PCBM/PMMA solution can be found in our previous report [21]. Perovskite solution is prepared by mixing FAI (1.1 M), PbI_2 (1.2 M), MABr (0.2 M) and $PbBr_2$ (0.2 M) in the mixture of DMF/DMSO (4:1 vol/vol). For the quadruple-cation, solution of RbI (30 μl) in DMSO (1.3 M) and solution of CsI (70 μl) in DMSO (1.3 M) are added into perovskite solution (1 ml). For the triple-cation, solution of CsI (100 μl) in DMSO (1.3 M) are added into perovskite solution (1 ml). In case of the dual-cation perovskite, the perovskite solution is prepared by mixing FAI (1.1 M), PbI_2 (1.1 M), CsBr (0.2 M) and $PbBr_2$ (0.2 M) in the mixture of DMF/DMSO (4:1 vol/vol). The perovskite film is spin-coated onto the sample with a 2-step program consisting of 2000 rpm for 10 s and 6000 rpm for 25 s. The sample is quickly transfered to a vacuum chamber and pumped down to low pressure (100–120 mTorr) for 10 s. The sample is then annealed at 100 °C for 30 min on a hotplate in case of quadruple-cation and triple-cation perovskite. In case of the dual-cation, the annealing condition is 50 min at 100 °C. PTAA solution (1 ml) is prepared by mixing the powder in toluene (10 mg/ml) with an additive of Li-TFSI (7.5 μl) in acetonitrile (170 mg/ml) and 4-tert-butylpyridine (tBP) (4 μl). The PTAA solution is spin-coated on the sample at 3000 rpm for 30 s with an acceleration rate of 3000 rpm/s. The CuPC solution is prepared by mixing the powder in chlorobenzene (10 mg/ml) with an additive of Li-TFSI (7.5 μl) in acetonitrile (170 mg/ml) and tBP (4 μl). The spinning condition for the CuPC is the same as for the PTAA. Finally a 100 nm of Au contact is deposited on the sample through a shadow mask by thermal evaporation for a cell active area of 0.16 cm^2.

To fabricate semi-transparent cells, the substrates go through the same processes as above up to the PTAA layer. Then 10 nm of MoO_x is deposited on the samples by thermal evaporation with a rate of 0.5 Å/s under a high vacuum (5×10^{-7} Torr). The rear transparent contact is then fabricated by sputtering 40 nm of IZO on the MoO_x. The sputtering is performed with 30 W of RF power with Ar pressure (1.5 mTorr) for 60 min. Au fingers are then deposited on the sample with a period of 1 mm and width of 30 μm (3% shading) using E-beam evaporation though a shadow mask.

2.3. Characterizations

The current − voltage characteristic of the cell is measured using Solar Simulator model SS150 equipped with a potentiostat source AutolabPGSTAT302N. The light intensity is calibrated at 1 sun (100 mW/cm^2, AM1.5 G) using the certified FraunhoferCalLab reference cell. The scan rate is fixed at 50 mV/s with a voltage step of 10 mV and a dwell time of 200 ms. The samples are put inside a temperature-controlled jig filled with constant flow of N2 and temperature controlled at 25 °C. Cross-sectional images are captured with Helios Nanolab 600 FIB system. Photoluminescence images of perovskite solar cells is taken following the procedure reported in our previous work [22]. In short, the illumination is provided by Lumileds blue light LEDs with a peak wavelength of emission of 450 nm filtered through Semrock FF01–451 band pass filters (400–500 nm). Images are captured using a Princeton Instruments Pixis 1024 camera with a Peltier-cooled (− 70 °C) silicon CCD detector. X-ray diffraction is performed with a D2 Phaser X-ray diffractometer with step size of 0.01° and integration time of 1 s per step. Cathodoluminescence (CL) measurement is performed on an FEI Verios scanning electron microscope (SEM) equipped with a GatanMonoCL4 Elite cathodoluminescence system. Perovskite samples for CL measurements are prepared on ITO/cp-TiO_2/ms-TiO_2 substrates, in which cp-TiO_2 stands for compact TiO_2 and ms-TiO_2 stands for mesoporous TiO_2. CL images are captured in panchromatic mode with appropriate dichroic filters. A long pass filter at 700 nm and band pass filter 500 ± 40 nm are used. The CL imaging is performed at a constant accelerating voltage of 5 kV with a beam current of 13pA. ToF-SIMS is

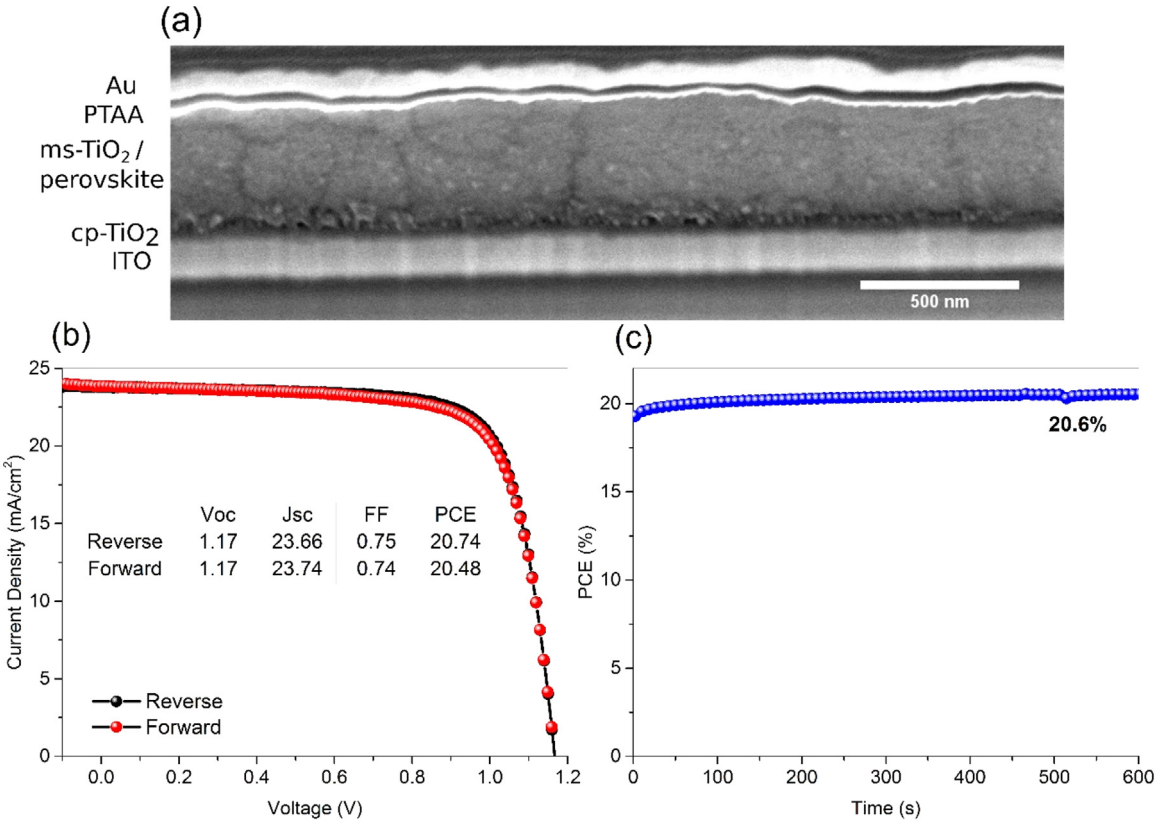

Fig. 1. (a) The structure of mesoporous PSCs using PTAA HTL in this study. (b) J-V scans of the champion cells in both reverse and forward directions with the scan rate of 50 mV/s. The inset shows the photovoltaic parameters extracted from the J-V curves. V_{oc} is the open circuit voltage, J_{sc} is the short circuit current density, FF is the fill factor and PCE is the power conversion efficiency of the cell. (c) Monitoring of the steady state efficiency of the champion cell at the V_{mpp} of 0.975 mV for 600 s.

performed using a dual beam depth profiling with Cs^+ primary ions for the erosion (1 keV, 75 nA) and primary beam Bi_3^+ for the analysis (15 keV, 0.4 pA). Light Beam Induced Current Mapping (LBIC) measurements are performed using a confocal WITec Alpha300 S scanning confocal microscope and a WhiteLase™ SC400 laser system. The scan area is fixed at the maximum 75 μm × 75 μm, which is limited by the stage movement of the system. The laser power is 8.2 μW and the laser spot diameter is 8 μm. Two excitation wavelengths are used for the LBIC measurement including 532 nm and 680 nm.

3. Results and discussion

3.1. Light and elevated temperature induced degradation (LeTID) in perovskite solar cells

We first show the cross-sectional SEM image of the PSCs used in this study (Fig. 1**a**). The cells employ a quadruple-cation perovskite composition $Rb_{0.03}Cs_{0.07}FA_{0.765}MA_{0.135}PbI_{2.55}Br_{0.45}$ (MA represents methylammonium) deposited using the vacuum-flash method as detailed in our previous work [23], The device structure is ITO/cp-TiO_2/ms-TiO_2/perovskite/PTAA/Au and the ms-TiO_2 layer is passivated by a thin layer of [6,6]-phenyl C61 butyric acid methyl ester (PCBM)/poly (methyl methacrylate) (PMMA). The champion cell has negligible hysteresis (Fig. 1**b**) and possesses a steady state efficiency of 20.6% (Fig. 1**c**), which is in-line with state-of-the-art PSCs using the same structure reported in literature. In comparison, the champion cell using the quadruple-cation perovskite and CuPC HTL has an efficiency of 19.06% (reverse scan) and 18.79% (forward scan) (Fig. S1), which is the highest value reported to date for this type of cell [12]. All the results presented next refer to PSCs employing PTAA HTL unless otherwise stated.

The thermal stability of the PSCs is studied when the cells are aged at 85 °C on a hotplate inside a glove box (O_2 level is less than 2 ppm) either in the dark or under illumination (using white LED illumination to give approximately 1 Sun intensity) for 16 h. We refer those aging conditions as “Under heat” and “Under light + heat”, respectively. In both cases, the cell temperature is measured using a thermocouple and the hotplate temperature is adjusted to give the same reading of 85 °C on the thermocouple. The efficiency of the cells is recorded at 25 °C before and after the aging test with the cells allowed to cool down for at least two hours prior to the measurement. Fig. 2**a** compares the photovoltaic parameters of two batches of cells normalized to their initial efficiencies. For the cells aged under heat only, there is a slight reduction in the V_{oc} and FF of the devices while the J_{sc} stays unchanged. As a result, PSCs aged under heat retain more than 95% of their initial efficiencies. This demonstrates that PSCs employing PTAA HTL are reasonably stable at 85 °C in the dark. On the other hand, efficiencies of PCSs aged under light + heat deteriorate significantly. On average, the V_{oc} decreases by more than 15%, the J_{sc} decreases by more than 24%, and the FF decreases by more than 28%. Subsequently, the cells retain only about 46% of their initial efficiency. Moreover, there is a big scatter in the photovoltaic parameters of the samples aged under light + heat, which suggests that multiple factors might have an impact on the cells in this aging condition. We also take photoluminescence (PL) images of the devices before and after the aging tests. Before the aging tests, both devices have uniform and comparable PL signals (Fig. S2). After the aging test, the device aged under heat has a much stronger and more uniform PL signal compared to the device aged under light + heat (Fig. 2**b, c**), which indicates that significant changes happen inside the cell. The same phenomenon is observed for PSCs employing CuPC as the HTL, where the performance slightly improves when the cells are under heat but drops to less than 40% of their initial

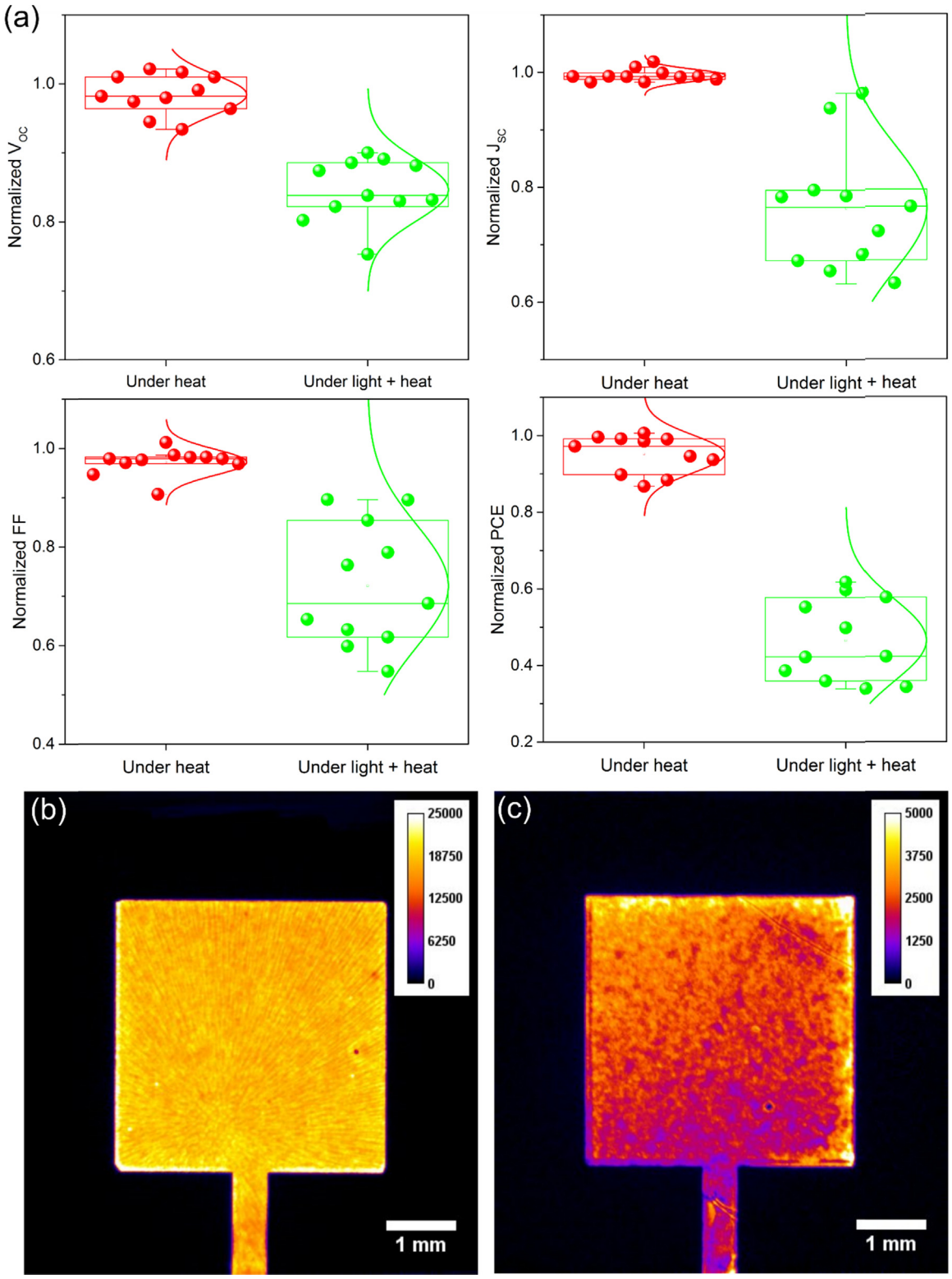

Fig. 2. (a) Comparison of two batches of cells (11 cells in each batch) undergoing thermal tests in dark and under light for 16 h in a N_2 environment. The graphs show the values of V_{OC}, J_{SC}, FF and PCE after the thermal tests normalized to the initial values. (b) PL image of a device aged under heat. (c) PL image of a device aged under light + heat. The active area is defined by the gold contact.

values when cells are aged under light + heat (Fig. S3a). PL images also reveal significant degradation in these cells when under light + heat (Fig. S3b,**c**). Furthermore, we perform LBIC measurements to understand more about the degradation mechanisms of PSCs under light + heat. This LBIC technique has been used to characterize the uniformity of the active layer in large area perovskite solar cells (PSCs) [24] and to study the degradation of PSCs in the presence of moisture [25,26]. As shown in Fig. S4, the photocurrents in the cell aged under heat in the dark are uniform (within one scan area and in different scan areas) are at similar level as the photocurrents in the fresh cell. In contrast, the

photocurrents in the cell aged under light + heat are much lower compared to the photocurrent in the fresh devices (Fig. S5). In addition, the photocurrents vary significantly in different scan area which indicates non-uniformity in the carrier collection efficiency in the device after being aged under light + heat. In this aging condition, the degradation is irreversible since the aged cells show no sign of recovery when tested again the next day after staying in the dark at room temperature overnight. This permanent degradation of PSCs due to the LeTID effect is of greater concern than the recoverable LeTID effect observed in silicon cells [15].

As the temperature is controlled at 85 °C when the PSCs are aged under heat or under light + heat, the observed difference should only come from the effect of light. We therefore test a device held at 25 °C under light (using white LED illumination at 1 Sun intensity) and find that the device experiences a slight enhancement in the performance, mainly in the FF, during operation for 16 h (Fig. S6). This means that light has no detrimental impact on the PSCs when they operate at 25 °C, but it has a severe impact once the cells operate at temperatures as low as 85 °C. We also test PSCs at different elevated temperatures including 50 °C, 60 °C and 70 °C under continuous illumination (using white LED illumination at 1 Sun intensity) and find that the cells perform stably at 50 °C and 60 °C for more than 43 h, however performance degrades notably and fluctuates when the cells operates at 70 °C (Fig. 3). However, the degradation of the cell operating at 70 °C is much less severe compared to when the cell operates at 85 °C. The LeTID effect is only triggered when the cell operates under light at temperatures above 60 °C. This also means that several standard qualification tests defined in the IEC-61646 including the damp heat and thermal cycling tests (where the devices are thermally aged in the dark), or light soaking (with the temperature range 50 +/−10 °C) might not guarantee the durability of PSCs.

3.2. Causes of LeTID in perovskite solar cells

To investigate the thermal instability of PSCs under light, we use X-ray diffraction (XRD) to scrutinize the effect of heat and light on the crystal structure of the perovskite active layer. The perovskite films are fabricated on ITO/cp-TiO_2/ms-TiO_2 substrates using the same method as in the cell structure. As shown in Fig. 4, the diffraction pattern is unchanged when the film is aged under heat. In contrast, there are some striking changes when the film is aged under light + heat. In particular, a new peak at 10.3° becomes notable, which indicates the formation of the Rb-rich phase. In addition, a peak at 12.7° emerges as a sign of the PbI_2 phase. Those changes clearly evidence the degradation of the perovskite film under light + heat for only 16 h. For a perovskite film exposed under ~ 1 Sun without intentional heating for 16 h, we find no change in the diffraction pattern. The diffraction pattern is also unchanged when the film is exposed to the light for 168 h as shown in Fig. S7. On the other hand, by prolonging the aging of the film under heat to 168 h, the PbI_2 peak at 12.7° becomes dominant over the perovskite peaks (Fig. S7) while the Rb-rich phase is negligible. This indicates that the significant decomposition of the quadruple-cation perovskite material is initiated by heat and accelerated by light while the segregation into the Rb-rich phase requires the combination of heat and light.

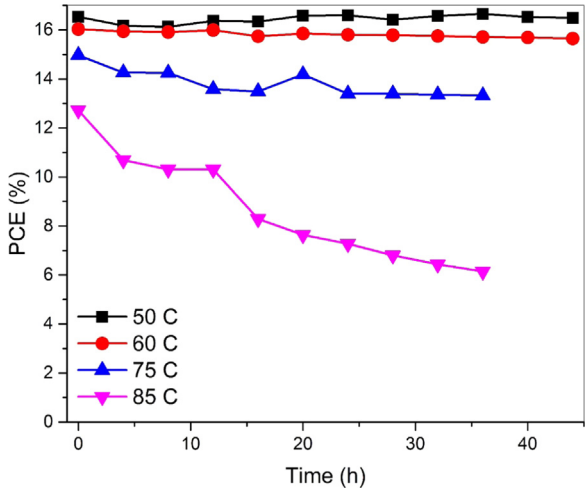

Fig. 3. The performance of PSCs monitored under continuous illumination at maximum power points and different temperatures.

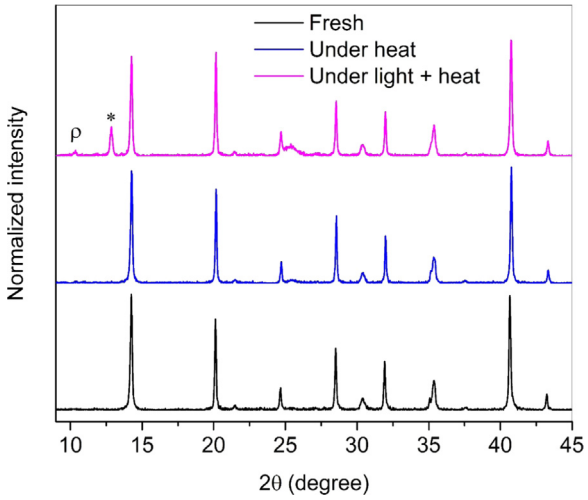

Fig. 4. XRD spectra of a fresh perovskite film and films exposed to different aging conditions: under heat and under light + heat for 16 h. The symbol ρ represents the Rb-rich phase while the symbol * represents the PbI_2 phase.

Scanning Electron Microscopy (SEM) and Cathodoluminescence (CL) imaging are effective methods to detect changes in the morphology and different phases on perovskite films as demonstrated in our previous report [27,28]. Using a long pass filter at 700 nm during the CL imaging, the perovskite phase is detected. When using a bandpass filter at 500 nm +/−40 nm, the PbI_2 and Rb-rich phases can be spatially resolved. As examined previously, the Rb-rich phase has a broadband CL spectrum peaking at ~ 570 nm while the PbI_2 phase has a narrow CL spectrum centered at ~ 515 nm. As a result, the PbI_2 phase will appear much brighter than the Rb-rich phase in a CL image with a bandpass filter of 500 nm +/−40 nm. As shown in Fig. 5, the fresh sample has a uniform perovskite phase with no Rb-rich phase and PbI_2 phase detected. The film aged under heat has slightly larger grain size due to the Ostwald ripening effect during heating. As for the fresh sample, the perovskite phase aged under heat is uniform and no Rb-rich phase or PbI_2 phase is observed. The perovskite film aged under light + heat also has slight larger grain size due to the effect of heat. However, there are some bright features with a size of a few micrometers in the SEM image. Those features appear dark in the CL image with the long pass filter and slightly bright in the CL image with the band pass filter. Those features have been confirmed as the Rb-rich phase using Energy Dispersive X-ray measurement (EDX) as shown in Fig. S8. Using a line scan measurement across the bright region, Rb is the only species whose atomic ratio increases significantly, from less than 2% outside of the region to 6–8% inside the region. There are some small bright spots in the band pass CL image, which indicate the presence of the PbI_2 phase. The SEM and CL images of a perovskite film aged under light for 16 h at room temperature are presented in Fig. S9 for consistency. The SEM picture shows no change in the grain size and the CL images show no presence of the Rb-rich phase or the PbI_2 phase. The SEM and CL results are consistent with the XRD results presented above, which confirms the decomposition of the perovskite film aged under light + heat into PbI_2 and the segregation of Rb into the Rb-rich phase. Owing to its small

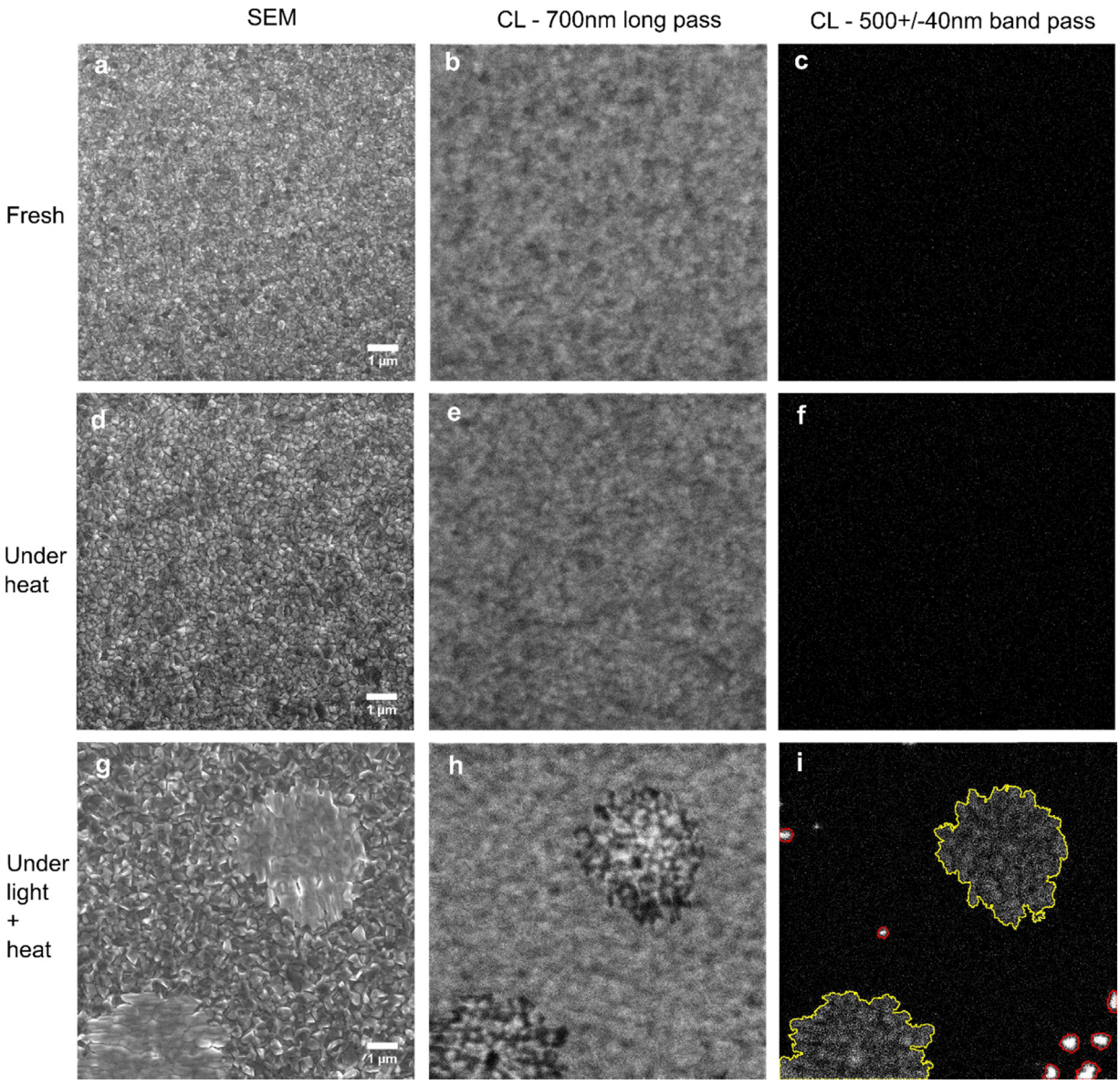

Fig. 5. SEM image, CL image with a long pass filter at 700 nm and CL image with a bandpass filter 500 + / − 40 nm of a fresh perovskite film (a-c), a perovskite film after aging under heat (d-f) and a perovskite film after aging under light + heat for 16 h (g-i). The yellow masks indicate the Rb-rich phase while the red masks indicate the PbI_2 phase.

ionic radius and considerable mismatch with the organic cations, Rb^+ is difficult to incorporate into the 3D perovskite and it is highly susceptible to phase segregation under external perturbation [29]. The addition of Rb negatively affects stability of the perovskite films under humidity due to the formation of the non-photoactive side product $RbPb_2I_4Br$ [30]. In fact, Ref. [24] even shows the appearance of Rb-rich phases on fresh samples, which later grow into clusters of Rb-rich phases with diameter ~ 100 µm after the sample has been exposed to 90% relative humidity for 20 h. In this work we show that, in the absence of moisture, Rb-rich phases also develop when samples are aged at 85 °C under light. The Rb-rich phases on the perovskite films can act as recombination centers, as confirmed by the dark spots in the CL image with the long pass filter and are therefore detrimental to the cell performance.

After identifying the effect of Rb on the light and thermal stability of the perovskite active layer, we remove Rb from the quadruple cation perovskite composition to form a triple-cation perovskite $Cs_{0.1}FA_{0.765}MA_{0.135}PbI_{2.55}Br_{0.45}$. Since the MA component has been reported to be intrinsically thermally unstable at 85 °C [31], we also go one step further to remove the MA component from the perovskite composition to eliminate potential degradation pathways. Therefore, the dual-cation perovskite composition $FA_{0.83}Cs_{0.17}Pb(I_{0.83}Br_{0.17})_3$ is also prepared.

We note that this composition has been used in previous reports in which PSCs are able to pass the damp heat test [4] and thermal cycling [32]. However, as mentioned before, those accelerated stress tests are only performed when PSCs are thermally aged in the dark. It is necessary to examine the robustness of the composition under the aging condition combining both heat and light to replicate the operating condition of photovoltaic modules in the field. We go through the same processes to investigate the light + heat stability of the perovskite films with triple-cation and dual-cation mixed-halide composition using XRD, SEM and CL. As shown in the supporting document (Supplementary Note 1 and Figs. S10-S13), we find that under the same aging condition, under 1 Sun light + 85 °C for 16 h, no Cs-rich phase is found. However, the formation of PbI_2 is still detected with some notable amount in the case of the triple-cation, and in a minor amount in the case of the dual-cation perovskite composition. The aging under

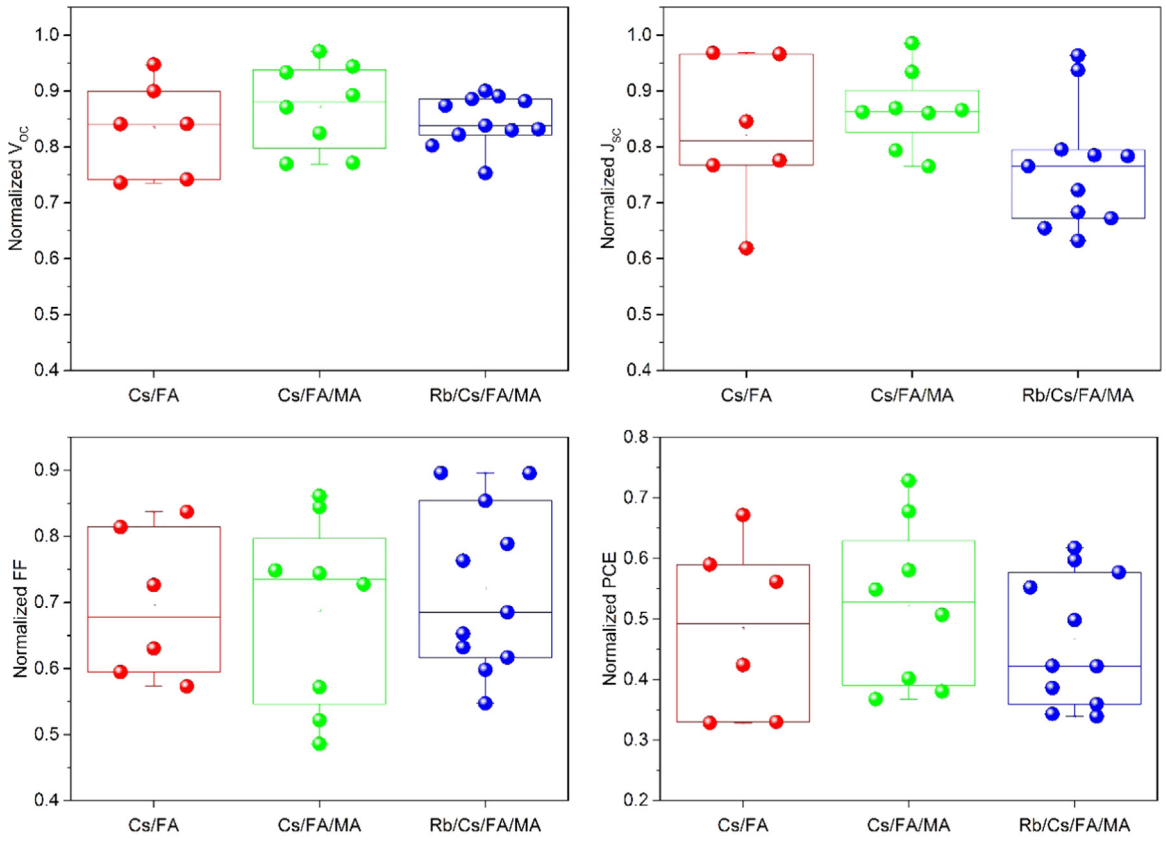

Fig. 6. Comparison of the stability of perovskites cells with three different perovskite composition: dual-cation, triple-cation and quadruple-cation. All the cells are aged under light + heat for 16 h. The graphs show the values of V_{OC}, J_{SC}, FF and PCE after the thermal tests normalized to the initial values.

heat is prolonged to 168 h for both the dual-cation and triple-cation perovskite composition. Similar to the quadruple-cation perovskite, the PbI_2 peak becomes the dominant peak for the triple-cation perovskite film, which indicates significant decomposition of the perovskite material. In contrast, a small PbI_2 peak is detected for the dual-cation perovskite film. The absorbance data shows some notable change for quadruple-cation and triple-cation, but only negligible change in the dual-cation perovskite (Fig. S14). The results prove that the presence of the MA cation in the perovskite composition makes it more susceptible to thermal decomposition at a temperature a low as 85 °C for long duration. We fabricate PSCs using those compositions to test the stability at the cell level. As shown in the Supplementary Note 2 and Figs. S15-S16, we achieve excellent efficiencies of over 20% for both the perovskite compositions, which prove the high quality of all the layers in our devices. We test the cells under light and heat to see if these compositions suffer from the LeTID effect and find that all the cells still degrade significantly (Fig. 6). Since the small PbI_2 phase emerging in the films after the aging test in the cases of triple-cation and dual-cation perovskite compositions cannot cause this severe drop in the performance [33,34], this phenomenon indicates that other factors are the main contributors to the degradation of the cells. We check the change in the conductivity of PTAA films deposited on quartz glasses before and after aging under light + heat. As shown in Fig. S17, the conductivity of PTAA is enhanced from 2.6 S cm^{-1} to 6.2 S cm^{-1} after 16 h under illumination at 85 °C and the conductivity remains unchanged when the aging duration is extended up to 96 h. Since PTAA is robust above 85 °C [35], the enhancement in the conductivity is most likely due to oxygen doping effect as demonstrated previously [36,37]. The oxygen may dope the PTAA during the conductivity measurement performed in the ambient atmosphere. As this enhancement is expected be beneficial for the cell performance, we exclude this as the cause of performance loss. We also exclude the possibility of degradation of the TiO_2 electron transport layer (ETL) under this condition since perovskite solar cells employing TiO_2 ETL and carbon electrode have been shown to be stable at 100 °C for 1500 h [38]. Therefore, the LeTID effect observed in the PSCs is likely to be linked to the degradation of the perovskite active layer or the interfaces between the active layer and ETL/HTL layers.

To elucidate the phenomenon, we use Time-of-Flight Secondary Ion Mass Spectrometry (ToF-SIMS) to map the distribution of different elements in the device before and after the aging tests. Fig. 7 shows the distribution of different elements as a function of sputter time, which is directly related to the depth below the gold contact surface. From the TOF-SIMS measurement, the CN^- signal is due to either the PTAA HTL

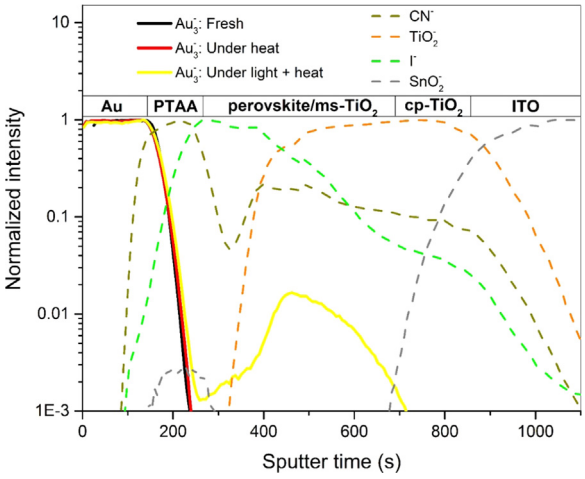

Fig. 7. TOF-SIMS analysis of a fresh sample, a sample aged under heat, and a sample aged under light + heat.

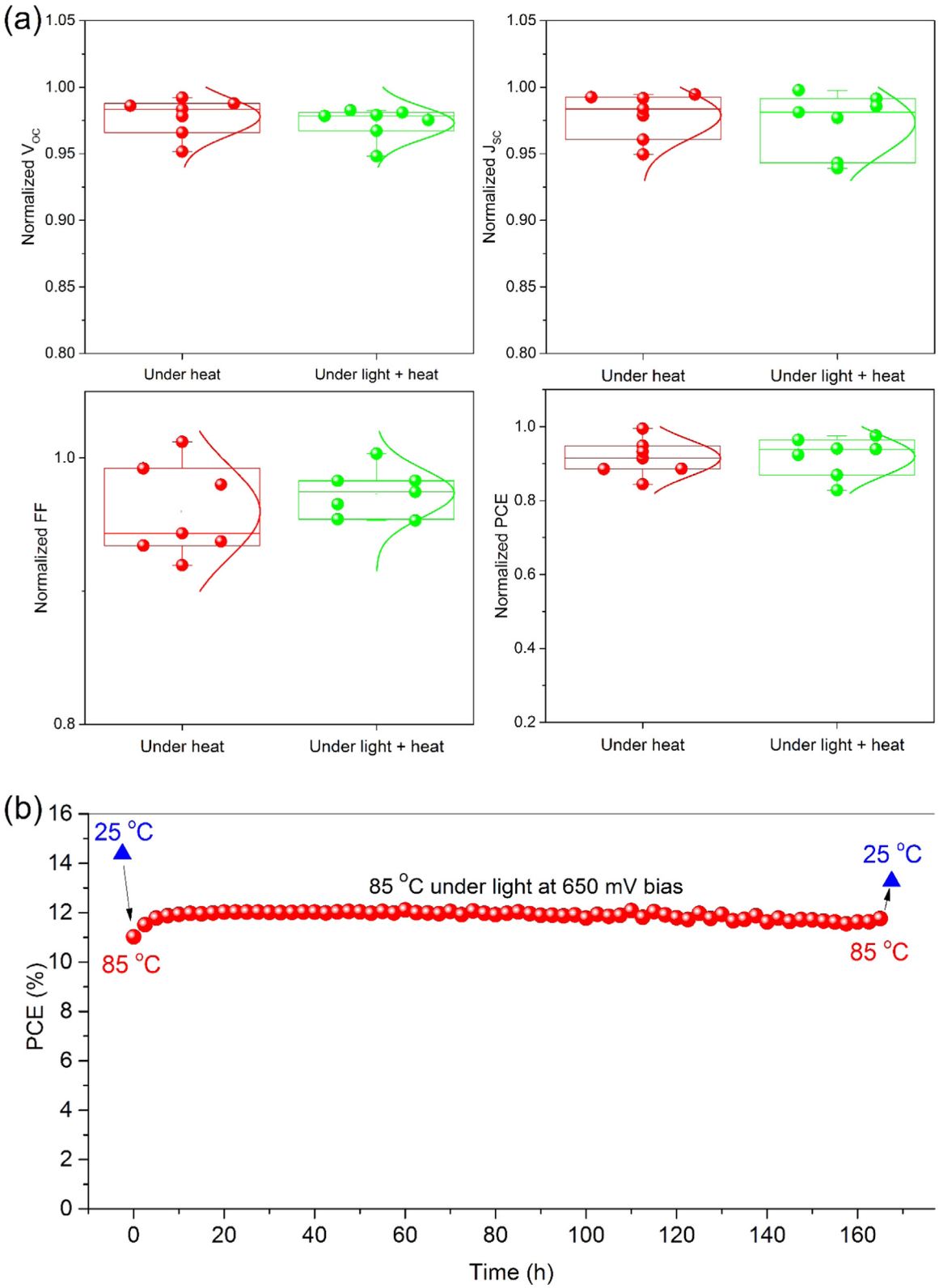

Fig. 8. (a) Comparison of two batches of semi-transparent cells (7 cells in each batch) undergoing thermal tests in dark and under light for 16 h in a N_2 environment. The graphs show the values of V_{OC}, J_{SC}, FF and PCE after the thermal tests normalized to the initial values. (b) Stability of semi-transparent PSC operate at 85 °C under light at 650 mV bias for 160 h.

or the perovskite active layer, while the I^- signal only comes from the perovskite layer. The TiO_2^- signal detects the appearance of the ms-TiO_2 and cp-TiO_2 electron transport layers. The SnO_2^- shows the location of the ITO front transparent contact on the device. The Au_3^- signal is used to identify the presence of elemental gold from the contact throughout the cross-section of the devices. In terms of the Au_3^- signal, the sample aged at 85 °C in the dark has a similar profile to the fresh sample. However, the sample aged at 85 °C under light has a remarkably

different Au_3^- profile. It is clear that the gold penetrates though the PTAA layer and into the perovskite active material in this case. This explains the reduction in the cell performance as well as in the PL signals when the cells are thermally aged under light as gold acts as a recombination center in the perovskite material. This phenomenon is the main contributing factor to the LeTID effect in PSCs. We note that the distribution of all other elements is the same for the three samples. The small SnO_2^- signal at the interface of Au and PTAA is currently under investigation. The diffusion of gold through a Spiro-MeOTAD HTL has been demonstrated for devices operating at 70 °C both in dark and under light [10], and under illumination at room temperature [39]. We have shown that PTAA can prevent the gold diffusion in PSCs only when the devices are aged at 85 °C in the dark or under illumination at room temperature, but not when simultaneously exposed to 85 °C and light. We speculate that the extra energy absorbed by the gold atoms when the device is aged under light activates the diffusion of gold through the PTAA layer at 85 °C. We also test the LeTID effect in PSCs employing Ag contact instead of Au contact. As shown in Fig. S18, we observe a similar LeTID effect in PSCs with Ag contact with the device degrading dramatically after aging under light at 85 °C while the performance drops moderately after aging in the dark at the same temperature. We note that the reaction of Ag and the iodide in the perovskite material might also contribute to the degradation of PSCs as reported previously [40].

3.3. Development of stable semi-transparent perovskite cells

To prevent the diffusion of gold when the device is operating at high temperature under light, we develop PSCs with a semi-transparent contact including a 10 nm thick MoO_x interlayer and a 40 nm thick indium doped zinc oxide (IZO). Gold fingers and bus bars are deposited on top of the IZO layer to improve the carrier collection. The devices have a high transparency of > 80% in the infrared and are thus promising for tandem applications with silicon cells. The dual-cation mixed halide perovskite composition $FA_{0.83}Cs_{0.17}Pb(I_{0.83}Br_{0.17})_3$ is used for the absorber. The top view photo and cross-sectional image of a PSC with semi-transparent contact is presented in Fig. S19. The efficiency of the PSC cells with semi-transparent contacts is lower than the normal cells with full area gold contact mainly due to a slightly lower J_{sc} and FF (Fig. 8).

We test the stability of semi-transparent PCSs in both conditions, under heat and under light + heat for 16 h. As shown in Fig. 6a, the semi-transparent cells show significantly improved stability against the LeTID effect as the cells retain more than 92% of the initial performance on average in both the aging conditions. We also prolong the test of the semi-transparent cell under light + heat and at 650 mV forward bias (close to the V_{MPP} of the cell at 85 °C) to simulate its operating condition at elevated temperatures. As shown in Fig. 6**b**, the cell operates stably at 85 °C for 160 h, and it recovers more than 90% of the initial efficiency after returning to 25 °C. The drop in the performance of semi-transparent cell is the results of a slight decrease in all photovoltaic parameters. The ToF-SIMS measurements on PSCs with semi-transparent contact and full gold contact on top indicates that the semi-transparent contact is effective in blocking the diffusion of gold into the perovskite active layer when the cell undergoes the light + heat aging for 16 h (Fig. S20). The results demonstrate that, by eliminating potential degradation pathways coming from gold diffusion and the Rb, the stability of PSCs against the LeTID effect can be significantly enhanced. In addition, we investigate the temperature coefficient of semi-transparent PSCs as shown in Fig. S21. As expected, efficiency decreases as the operating temperature increases and the temperature coefficient of the semi-transparent cell is calculated to be − 0.45% °C^{-1} in the temperature range 25–85 °C. As compared to silicon cells with a P_{MAX} temperature coefficient in the range of − 0.3 to − 0.5% °C^{-1}, the semi-transparent cell has a similar temperature coefficient [41]. Further study is required to understand the slight drop in the performance of PSCs with semi-transparent contacts after the aging test. One possibility is the use of MoO_x as the interlayer since reaction between the perovskite and MoO_x has been reported [42]. This issue could be resolved by using an ITO nanoparticle interlayer as in previous reports [43,44]. Furthermore, the exact onset temperature, formation rates and activation energies of the LeTID effect in PSCs with full gold contact need to be investigated in more detail. It would also be interesting to examine the LeTID effect in PSCs with different cell structures such as inverted cells and cells with carbon electrode.

4. Conclusion

In conclusion, we have shown that light has a detrimental impact on the thermal stability of PSCs mainly due to the light-activated diffusion of gold through the HTL layer into the perovskite layer. In addition, the Rb in the quadruple-cation mixed-halide perovskite segregates into Rb-rich phases under the aging condition combining both light and heat. This severe LeTID effect in PSCs requires modification to the existing IEC-61646 testing standard for early failure detection. To enhance the robustness of PSCs against the LeTID effect, we develop PSCs with semi-transparent contacts and stable perovskite composition which show improved stability when operating at 85 °C under light for more than 160 h.

Acknowledgements

This work has been supported by the Australian Government through the Australian Renewable Energy Agency (ARENA). Responsibility for the views, information or advice expressed herein is not accepted by the Australian Government. Part of the experiment was performed at Australian National Fabrication Facility (ANFF) ACT Node. TD acknowledges the support of a Postdoc Fellowship from the Australian Centre for Advanced Photovoltaics (ACAP). KRC acknowledges the support of a Future Fellowship from the Australian Research Council.

Appendix A. Supporting information

Supplementary data associated with this article can be found in the online version at doi:10.1016/j.solmat.2018.08.017

References

[1] A. Kojima, K. Teshima, Y. Shirai, T. Miyasaka, Organometal halide perovskites as visible-light sensitizers for photovoltaic cells, J. Am. Chem. Soc. 131 (2009) 6050–6051.
[2] W.S. Yang, B.-W. Park, E.H. Jung, N.J. Jeon, Y.C. Kim, D.U. Lee, S.S. Shin, J. Seo, E.K. Kim, J.H. Noh, S.I. Seok, Iodide management in formamidinium-lead-halide–based perovskite layers for efficient solar cells, Science 356 (2017) 1376–1379.
[3] T. Duong, Y. Wu, H. Shen, J. Peng, X. Fu, D. Jacobs, E.C. Wang, T.C. Kho, K.C. Fong, M. Stocks, E. Franklin, A. Blakers, N. Zin, K. McIntosh, W. Li, Y.B. Cheng, T.P. White, K. Weber, K. Catchpole, Rubidium multication perovskite with optimized bandgap for perovskite-silicon tandem with over 26% efficiency, Adv. Energy Mater. 7 (2017) 1700228.
[4] K.A. Bush, A.F. Palmstrom, Z.J. Yu, M. Boccard, R. Cheacharoen, J.P. Mailoa, D.P. McMeekin, R.L.Z. Hoye, C.D. Bailie, T. Leijtens, I.M. Peters, M.C. Minichetti, N. Rolston, R. Prasanna, S. Sofia, D. Harwood, W. Ma, F. Moghadam, H.J. Snaith, T. Buonassisi, Z.C. Holman, S.F. Bent, M.D. McGehee, 23.6%-efficient monolithic perovskite/silicon tandem solar cells with improved stability, Nat. Energy 2 (2017) 17009.
[5] T. Sherahilo, Oxford PV sets world record for perovskite solar cell, 2018.
[6] T. Leijtens, G.E. Eperon, N.K. Noel, S.N. Habisreutinger, A. Petrozza, H.J. Snaith, Stability of metal halide perovskite solar cells, Adv. Energy Mater. 5 (2015) 1500963.
[7] X. Li, M. Tschumi, H. Han, S.S. Babkair, R.A. Alzubaydi, A.A. Ansari, S.S. Habib, M.K. Nazeeruddin, S.M. Zakeeruddin, M. Grätzel, Outdoor performance and stability under elevated temperatures and long-term light soaking of triple-layer mesoporous perovskite photovoltaics, Energy Technol. 3 (2015) 551–555.
[8] X. Zhao, H.-S. Kim, J.-Y. Seo, N.-G. Park, Effect of selective contacts on the thermal stability of perovskite solar cells, ACS Appl. Mater. Interfaces 9 (2017) 7148–7153.
[9] C.D. Bailie, E.L. Unger, S.M. Zakeeruddin, M. Gratzel, M.D. McGehee, Melt-infiltration of spiroOMeTAD and thermal instability of solid-state dye-sensitized solar

cells, Phys. Chem. Chem. Phys. 16 (2014) 4864–4870.
[10] K. Domanski, J.-P. Correa-Baena, N. Mine, M.K. Nazeeruddin, A. Abate, M. Saliba, W. Tress, A. Hagfeldt, M. Grätzel, Not all that glitters is gold: metal migration-induced degradation in perovskite solar cells, ACS Nano (2016).
[11] L. Shi, T.L. Young, J. Kim, Y. Sheng, L. Wang, Y. Chen, Z. Feng, M.J. Keevers, X. Hao, P.J. Verlinden, M.A. Green, A.W.Y. Ho-Baillie, Accelerated lifetime testing of organic–inorganic perovskite solar cells encapsulated by polyisobutylene, ACS Appl. Mater. Interfaces 9 (2017) 25073–25081.
[12] Y.C. Kim, T.Y. Yang, N.J. Jeon, J. Im, S. Jang, T.J. Shin, H.W. Shin, S. Kim, E. Lee, S. Kim, J.H. Noh, S.I. Seok, J. Seo, Engineering interface structures between lead halide perovskite and copper phthalocyanine for efficient and stable perovskite solar cells, Energy Environ. Sci. 10 (2017) 2109–2116.
[13] R. Arndt, R. Puto, Basic understanding of IEC standard testing for photovoltaic panels, Compliance Mag. (2010).
[14] F. Kersten, P. Engelhart, H.-C. Ploigt, A. Stekolnikov, T. Lindner, F. Stenzel, M. Bartzsch, A. Szpeth, K. Petter, J. Heitmann, J.W. Müller, Degradation of multicrystalline silicon solar cells and modules after illumination at elevated temperature, Sol. Energy Mater. Sol. Cells 142 (2015) 83–86.
[15] F. Kersten, F. Fertig, K. Petter, B. Klöter, E. Herzog, M.B. Strobel, J. Heitmann, J.W. Müller, System performance loss due to LeTID, Energy Procedia 124 (2017) 540–546.
[16] F. Fertig, K. Krauß, S. Rein, Light-induced degradation of PECVD aluminium oxide passivated silicon solar cells, Phys. Status Solidi RRL 9 (2015) 41–46.
[17] F. Fertig, R. Lantzsch, A. Mohr, M. Schaper, M. Bartzsch, D. Wissen, F. Kersten, A. Mette, S. Peters, A. Eidner, J. Cieslak, K. Duncker, M. Junghänel, E. Jarzembowski, M. Kauert, B. Faulwetter-Quandt, D. Meißner, B. Reiche, S. Geißler, S. Hörnlein, C. Klenke, L. Niebergall, A. Schönmann, A. Weihrauch, F. Stenzel, A. Hofmann, T. Rudolph, A. Schwabedissen, M. Gundermann, M. Fischer, J.W. Müller, D.J.W. Jeong, Mass production of p-type Cz silicon solar cells approaching average stable conversion efficiencies of 22%, Energy Procedia 124 (2017) 338–345.
[18] N. Tim, S. Florian, K. Wolfram, E. Rebekka, S. Jonas, M.C. Schubert, Understanding the light-induced degradation at elevated temperatures: Similarities between multicrystalline and floatzone p-type silicon, Prog. Photovolt. (2017).
[19] Z. Annika, S. Daniel, H. Giso, Degradation and regeneration in mc-Si after different gettering steps, Prog. Photovolt. 25 (2017) 545–552.
[20] R. Eberle, W. Kwapil, F. Schindler, S.W. Glunz, M.C. Schubert, Firing temperature profile impact on light induced degradation in multicrystalline silicon, Energy Procedia 124 (2017) 712–717.
[21] J. Peng, Y. Wu, W. Ye, D.A. Jacobs, H. Shen, X. Fu, Y. Wan, T. Duong, N. Wu, C. Barugkin, H.T. Nguyen, D. Zhong, J. Li, T. Lu, Y. Liu, M.N. Lockrey, K.J. Weber, K.R. Catchpole, T.P. White, Interface passivation using ultrathin polymer-fullerene films for high-efficiency perovskite solar cells with negligible hysteresis, Energy Environ. Sci. 10 (2017) 1792–1800.
[22] D. Walter, Y. Wu, T. Duong, J. Peng, L. Jiang, K.C. Fong, K. Weber, On the use of luminescence intensity images for quantified characterization of perovskite solar cells: spatial distribution of series resistance, Adv. Energy Mater. 8 (2018) 1701522.
[23] Y. Wu, D. Yan, J. Peng, T. Duong, Y. Wan, S.P. Phang, H. Shen, N. Wu, C. Barugkin, X. Fu, S. Surve, D. Grant, D. Walter, T.P. White, K.R. Catchpole, K.J. Weber, Monolithic perovskite/silicon-homojunction tandem solar cell with over 22% efficiency, Energy Environ. Sci. 10 (2017) 2472–2479.
[24] S. Razza, F. Di Giacomo, F. Matteocci, L. Cinà, A.L. Palma, S. Casaluci, P. Cameron, A. D'Epifanio, S. Licoccia, A. Reale, T.M. Brown, A. Di Carlo, Perovskite solar cells and large area modules (100cm2) based on an air flow-assisted PbI2 blade coating deposition process, J. Power Sources 277 (2015) 286–291.
[25] Z. Song, A. Abate, S.C. Watthage, G.K. Liyanage, A.B. Phillips, U. Steiner, M. Graetzel, M.J. Heben, Perovskite solar cell stability in humid air: partially reversible phase transitions in the PbI2-CH3NH3I-H2O system, Adv. Energy Mater. 6 (2016) 1600846.
[26] Y. Yao, G. Wang, F. Wu, D. Liu, C. Lin, X. Rao, R. Wu, G. Zhou, Q. Song, The interface degradation of planar organic–inorganic perovskite solar cell traced by light beam induced current (LBIC), RSC Adv. 7 (2017) 42973–42978.
[27] T. Duong, H.K. Mulmudi, H. Shen, Y. Wu, C. Barugkin, Y.O. Mayon, H.T. Nguyen, D. Macdonald, J. Peng, M. Lockrey, W. Li, Y.-B. Cheng, T.P. White, K. Weber, K. Catchpole, Structural engineering using rubidium iodide as a dopant under excess lead iodide conditions for high efficiency and stable perovskites, Nat. Energy 30 (2016) 330–340.
[28] T. Duong, H.K. Mulmudi, Y. Wu, X. Fu, H. Shen, J. Peng, N. Wu, H.T. Nguyen, D. Macdonald, M. Lockrey, T.P. White, K. Weber, K. Catchpole, Light and electrically induced phase segregation and its impact on the stability of quadruple cation high bandgap perovskite solar cells, ACS Appl. Mater. Interfaces 9 (2017) 26859–26866.
[29] D.J. Kubicki, D. Prochowicz, A. Hofstetter, S.M. Zakeeruddin, M. Grätzel, L. Emsley, Phase segregation in Cs-, Rb-and K-doped mixed-cation (MA) x (FA) 1–x PbI3 hybrid perovskites from solid-state NMR, J. Am. Chem. Soc. 139 (2017) 14173–14180.
[30] Y. Hu, M.F. Aygüler, M.L. Petrus, T. Bein, P. Docampo, Impact of rubidium and cesium cations on the moisture stability of multiple-cation mixed-halide perovskites, ACS Energy Lett. 2 (2017) 2212–2218.
[31] B. Conings, J. Drijkoningen, N. Gauquelin, A. Babayigit, J. D'Haen, L. D'Olieslaeger, A. Ethirajan, J. Verbeeck, J. Manca, E. Mosconi, F.D. Angelis, H.G. Boyen, Intrinsic thermal instability of methylammonium lead trihalide perovskite, Adv. Energy Mater. 5 (2015) 1500477.
[32] R. Cheacharoen, N. Rolston, D. Harwood, K.A. Bush, R.H. Dauskardt, M.D. McGehee, Design and understanding of encapsulated perovskite solar cells to withstand temperature cycling, Energy Environ. Sci. 11 (2018) 144–150.
[33] Y.C. Kim, N.J. Jeon, J.H. Noh, W.S. Yang, J. Seo, J.S. Yun, A. Ho-Baillie, S. Huang, M.A. Green, J. Seidel, T.K. Ahn, S.I. Seok, Beneficial effects of PbI2 incorporated in organo-lead halide perovskite solar cells, Adv. Energy Mater. 6 (2016) 1502104.
[34] D. Bi, W. Tress, M.I. Dar, P. Gao, J. Luo, C. Renevier, K. Schenk, A. Abate, F. Giordano, J.-P.C. Baena, Efficient luminescent solar cells based on tailored mixed-cation perovskites, Sci. Adv. 2 (2016) e1501170.
[35] M. Saliba, T. Matsui, K. Domanski, J.-Y. Seo, A. Ummadisingu, S.M. Zakeeruddin, J.-P. Correa-Baena, W.R. Tress, A. Abate, A. Hagfeldt, M. Grätzel, Incorporation of rubidium cations into perovskite solar cells improves photovoltaic performance, Science 354 (2016) 206–209.
[36] U.B. Cappel, T. Daeneke, U. Bach, Oxygen-induced doping of spiro-MeOTAD in solid-state dye-sensitized solar cells and its impact on device performance, Nano Lett. 12 (2012) 4925–4931.
[37] Z. Hawash, L.K. Ono, Y. Qi, Moisture and oxygen enhance conductivity of LiTFSI-doped spiro-MeOTAD hole transport layer in perovskite solar cells, Adv. Mater. Interfaces 3 (2016) 1600117.
[38] A.K. Baranwal, K. Shusaku, P.T.A. Nirmal, M. Gai, N. Tomoya, K. Hiroyuki, M. Tsutomu, S. Hiroshi, I. Seigo, 100 °C thermal stability of printable perovskite solar cells using porous carbon counter electrodes, ChemSusChem 9 (2016) 2604–2608.
[39] S. Cacovich, L. Ciná, F. Matteocci, G. Divitini, P. Midgley, A. Di Carlo, C. Ducati, Gold and iodine diffusion in large area perovskite solar cells under illumination, Nanoscale 9 (2017) 4700–4706.
[40] K. Yuichi, L.K. Ono, M.V. Lee, Shenghao Wang, S.R. Raga, Y. Qi, Silver iodide formation in methyl ammonium lead iodide perovskite solar cells with silver top electrodes, Adv. Mater. Interfaces 2 (2015) 1500195.
[41] E. Skoplaki, J.A. Palyvos, On the temperature dependence of photovoltaic module electrical performance: a review of efficiency/power correlations, Sol. Energy 83 (2009) 614–624.
[42] E.S. Thibau, A. Llanos, Z.-H. Lu, Disruptive and reactive interface formation of molybdenum trioxide on organometal trihalide perovskite, Appl. Phys. Lett. 110 (2017) 081604.
[43] D.P. McMeekin, G. Sadoughi, W. Rehman, G.E. Eperon, M. Saliba, M.T. Hörantner, A. Haghighirad, N. Sakai, L. Korte, B. Rech, M.B. Johnston, L.M. Herz, H.J. Snaith, A mixed-cation lead mixed-halide perovskite absorber for tandem solar cells, Science 351 (2016) 151–155.
[44] K.A. Bush, C.D. Bailie, Y. Chen, A.R. Bowring, W. Wang, W. Ma, T. Leijtens, F. Moghadam, M.D. McGehee, Thermal and environmental stability of semi--transparent perovskite solar cells for tandems enabled by a solution-processed nanoparticle buffer layer and sputtered ITO electrode, Adv. Mater. 28 (2016) 3937–3943.